

HIGH-RESOLUTION SPECTROSCOPIC X-RAY DIAGNOSTICS FOR STUDYING THE ION KINETIC ENERGY AND PLASMA PROPERTIES IN A Z-PINCH AT STAGNATION

E. Kroupp[‡], D. Carasso, D. Osin, A. Starobinets, V. Bernshtam, V. Fisher, Yu. Ralchenko, Yu. Zarnitsky and Y. Maron

Faculty of Physics, Weizmann Institute of Science, Rehovot, Israel

I. Uschmann, and E. Förster

Friedrich-Schiller Universität, Jena, Germany

A. Fisher

Faculty of Physics, Technion-Israeli Institute of Technology, Haifa, Israel

Abstract

Doubly-curved-crystal spectroscopic systems are used to obtain time-resolved measurements of Ne K emission from the stagnating plasma in a Ne-puff Z-pinch experiment. These systems, with a spectral resolving power of $\cong 6700$ (only limited by the crystal Rocking curve) and simultaneous z-imaging with a resolution $\cong 0.1$ mm, are used to obtain the time history of the ion kinetic energy at stagnation from the line profiles of Ly α satellites, which were verified to be optically thin. The measurements allowed for tracking the ion energy throughout the entire K-emission period. It was found that the ions lose most of their kinetic energy during the K-emission period, i.e. before the electrons cool down enough to terminate the K-emission, and before the ions recombine to Li-like charge state. Also in this study, the profile of the optically thin intercombination line was used to investigate the velocities of the He-like ions. Together with the determination of the electron density from satellite ratios, absolute line and continuum intensities, time resolved observation of the plasma size, and collisional-radiative and radiation-transport calculations, these data are used to study the various contributions to the energy deposition and energy losses of the plasma at stagnation.

I. INTRODUCTION

Investigations of the energy transfer from the imploding plasma to the electrons at the stagnation phase in a Z-pinch experiment are essential for studying the thermalization processes at the pinch column, and for the progress towards the understanding of the pinch-formation dynamics. For such investigations, an experimental determination of the ion velocity distribution as a function of time throughout the stagnation phase is of decisive importance. Such measurements can be performed if ionic line-emission

with Doppler-dominated spectral profiles are detected. A principal requirement for such measurements is, therefore, that the line profiles are not affected by the line opacity, while the line intensity is sufficiently high to allow for a satisfactory signal-to-noise ratio in the line-profile measurements. In addition, the line profile should not be significantly affected by the Stark broadening. Furthermore, the instrumental spectral resolution must not limit the accuracy of the line-profile measurements. Measurements of Doppler contributions to line profiles for studying the ion kinetic energy in the stagnating plasma was reported in Refs. [1,2,3].

In this study we report on a time-resolved determination of the ion kinetic energy in a stagnating plasma in a gas-puff neon Z-pinch experiment. Measurements of the kinetic energy, performed in different experiments for different times throughout the entire x-ray emission period, allow for tracking the history of the ion kinetic energy. For these measurements we selected lines (Ly α satellites) that, using radiation transport calculations, were verified to be free of opacity effects and, using Stark broadening calculations, were found to be insignificantly affected by Stark broadening. Also, we developed spectroscopic systems that provide rather high spectral resolution ($\lambda/\Delta\lambda \cong 6700$), which is evidently essential for such measurements. Furthermore, the spectroscopic systems employed allow for a simultaneous imaging the pinch column along its z axis, which provided information that is highly important for the data analysis. The data demonstrate that the ions lose most of their kinetic energy, reaching an energy comparable to the electron temperature, during the x-ray emission period.

II. EXPERIMENTAL SYSTEM AND DIAGNOSTICS

The gas in the present experiments is injected by two nozzles on the cathode side, where one is annular with a diameter of 38 mm delivering a gas load of $\cong 18$ $\mu\text{g}/\text{cm}$,

[‡] email: fnkroupp@plasma-gate.weizmann.ac.il

and the other is on axis, delivering $\cong 4 \mu\text{g}/\text{cm}$. The implosion time is $\sim 750 \text{ ns}$, and the current at stagnation is $\cong 320 \text{ kA}$.

The main features of the spectroscopic systems developed for this study are the high spectral resolution ($\lambda/\Delta\lambda \cong 6700$) and the spatial imaging of the spectra with a resolution down to 0.1 mm . Single-gated MCP detectors followed by CCD cameras, provide 2-ns temporal resolution throughout the 20-ns x-ray emission period.

The crystal used for this study is a spherically curved KAP operated at the second order. Using double-grating measurements it was verified that the spectrograph-system spectral resolution is only limited by the crystal rocking curve. Employing a high-dispersion for the spectrograph ($R=612 \text{ mm}$) allowed for resolving the crystal rocking curve at the detector plane, giving a resolving power $\cong 6700$ (i.e., the Lorentzian spectral response is $1.8 \text{ m}\text{\AA}$ wide) and providing a spectral window of $60\text{-}100 \text{ m}\text{\AA}$. We also note that possible instrumental broadening due to the pinch size was shown to be negligible in the present measurements.

In order to measure the Doppler profiles in the stagnation phase, the crystal was designed to focus on three Ne Ly α satellites ($12.310\text{-}12.355 \text{ \AA}$). In addition, a pinhole-photography system was used to provide filtered 2-D images of the pinch column at four gated times ($\geq 1 \text{ ns}$ delay between each gate). The other diagnostic tools included x-ray diodes (XRD) and a system of Ross filters [4], equipped with fast PIN-diode detectors.

III. MEASUREMENTS AND RESULTS

The satellites observed in this study are [5,6]: $2p^2 \ ^1D_2\text{-}1s2p \ ^1P_1$, $2s2p \ ^3P_{0,1,2}\text{-}1s2s \ ^3S_1$, and $2p^2 \ ^3P_{0,1,2}\text{-}1s2p \ ^3P_{0,1,2}$ where one is a singlet transition (12.355 \AA) and the other two are triplet transitions with three components (between 12.305 to 12.310 \AA) and six components (between 12.321 to 12.326 \AA), respectively. Due to its relatively simpler spectral profile, the satellite most useful for the ion-velocity measurements is the singlet one. For our plasma parameters, the natural (Lorentzian) broadening of this line is mainly determined by the rates of the upper-level autoionization ($3.7 \times 10^{14} \text{ s}^{-1}$) and the radiative-decay ($1.2 \times 10^{13} \text{ s}^{-1}$), giving a natural width of $3.3 \text{ m}\text{\AA}$. This width, together with the instrumental spectral response ($1.8 \text{ m}\text{\AA}$), determine the spectral resolution for these observations.

Employing the z-imaging described above for these Ly α satellites revealed that they are first emitted from the region $z=9\text{-}12 \text{ mm}$, where $z=0$ and $z=14.4 \text{ mm}$ are the cathode and anode positions, respectively. We now discuss the measurements for this region.

Figure 1 shows an example of the satellite structure observed at a relatively early time of the x-ray emission period, $t=-3 \text{ ns}$, where $t=0$ denotes the peak time of the XRD detector that collects $> 800 \text{ eV}$ photons from the

entire pinch column. The resulting satellite profiles at $z=10.5 \text{ mm}$, and integrated over $\Delta z=1.6 \text{ mm}$, are shown in Figure 2. In order to obtain the Doppler contribution to the line width we assume a Gaussian shape for this contribution, where the other contributions are due to the Lorentzian natural broadening and instrumental response. We thus fit Voigt profiles to each of the satellite components, where the Gaussian part is a parameter determined by the best fit. For the early time of the stagnation, the data give that the width (FWHM) of the Gaussian contribution to the profiles of the singlet satellite is between 8 and $11 \text{ m}\text{\AA}$ (significantly larger than the natural width and the instrumental response width). The widths observed can only be associated with the Doppler effect, resulting from the ion thermal and hydrodynamic velocities. Indeed, assuming that each component of the other triplet satellites observed has the same width as the singlet satellite (consistent with Doppler-dominated widths), it was possible to reconstruct reasonably well the satellite structure of the triplet satellites, as show in Figure 2.

For later times the line emission was seen from the z region between $z=6$ and 14.4 mm . Here, we only discuss the late emission from the region $z=9\text{-}12 \text{ mm}$, thus only addressing the time dependence of the ion kinetic energies at this region. An example of a satellite structure observed later in the stagnation is shown in Figure 3. It is seen that the Gaussian FWHM at $t=6 \text{ ns}$ is $2.5 \pm 0.6 \text{ m}\text{\AA}$. The Doppler contribution in this example corresponds to an ion temperature of $140 \pm 75 \text{ eV}$. This is perhaps the lowest ion temperature expected to be detected since very plausibly the ions cannot be much colder than the electrons. Indeed, at this period of the stagnation the electron temperature is $< 200 \text{ eV}$ (which will be discussed elsewhere), demonstrating that the mean ion kinetic energy is tracked in our experiments down to Te .

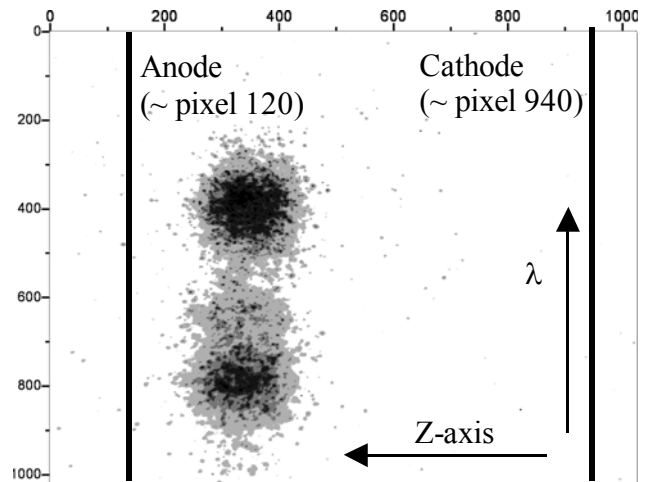


Figure 1. The Ly α satellites imaged in the z-direction observed at $t=-3 \text{ ns}$ (relative to the XRD-signal peak time) with a 2-ns gated MCP camera. The scales are in pixel number on the CCD camera.

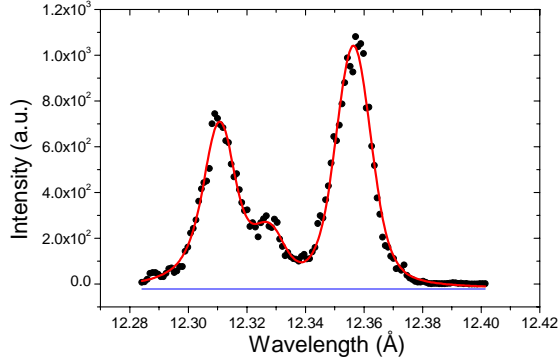


Figure 2. Satellite spectrum for $z=10.5$ mm, integrated over $\Delta z=1.6$ mm, for $t=-3$ ns.

It is noteworthy that the observation of the ion kinetic energy down to the electron temperature, with a Gaussian contribution to the line profile of 2.5 mÅ, was only possible due to the high spectral resolution (~ 4 mÅ, see above) achieved for the present measurements.

The measured FWHM of the Gaussian contributions for $z=9$ to 12 mm as a function of time are summarized in Figure 4. The error bars shown are mainly due to the shot-to-shot irreproducibility for the same time gate.

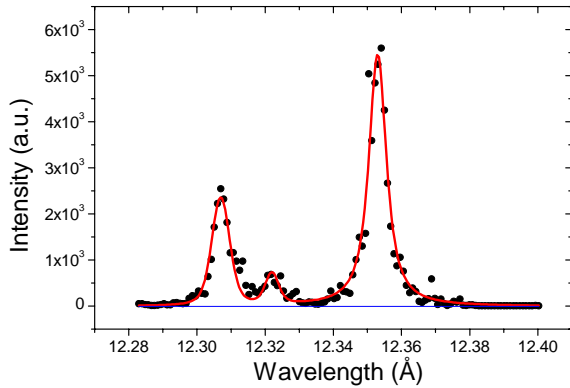


Figure 3. Satellite spectrum observed at $z=10$ mm and integrated over $\Delta z=0.2$ mm for $t=6$ ns. The best-fit-Gaussian FWHM is 2.5 ± 0.6 mÅ.

The data presented above are also used to obtain rather reliably the electron density $n_e(H)$ in the H-like plasma at stagnation. As discussed below, the $2121'$ doubly-excited levels are primarily populated by dielectronic recombination and depopulated by autoionizations and radiative decays. However, the ratio between the populations of the $2p^2\ ^3P$ autoionizing-level and the upper levels of the other two satellites observed depends on $n_e(H)$, due to the rise of the $2p^2\ ^3P$ population with $n_e(H)$ that results from the collisional mixing of the levels.

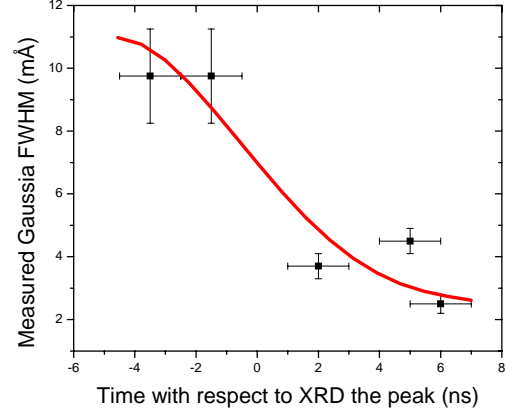


Figure 4. The time dependence of the Gaussian FWHM, averaged over different shots and over regions of 0.2 to 1.6 mm around $z=10.5$ mm. The curve indicates the trend.

We thus use the observed intensity ratios of the satellites given above, together with our atomic-physics modeling, to determine $n_e(H)$ in the plasma. It is noteworthy that here we assumed that the $Ly\alpha$ -satellite Doppler widths yield the H-like ion energy. This is fully correct if the satellite lines observed are due to dielectronic capture (rather than due to inner-shell excitations). Our calculations indicate that this is the case for Maxwellian electrons, while for nonMaxwellian electrons the analysis is still in progress. Sensitivities to fast changes in T_e are also currently studied.

IV. DISCUSSION

A detailed analysis of the data presented above will be given in a separate publication. Here, we only describe the modeling required for elucidating the physics processes provided by these data.

The measurements give the total kinetic energy of the H-like ions throughout the $Ly\alpha$ -emission period ($t \cong -4$ to $t \cong +6$ ns relative to the XRD-signal peak). The kinetic energy of the ions at the final phase of the implosion (prior to the $Ly\alpha$ emission, i.e., prior to the occurrence of the ionization processes at the stagnation phase) may be higher than observed at $t \cong -4$ ns, since possibly some fraction of the ion energy prior to stagnation is dissipated on the ionization processes that lead to the early formation of the H-like ions. Here, we only consider the ion kinetic energy at the $Ly\alpha$ -emission period and discuss the energy balance at this period.

As the imploding ions reach the axis region in the z -pinch, the ions tend to thermalize due to the high-rate ion-ion collisionality in this region, resulting from the relatively high density there. An analysis of the ion thermalization processes in the stagnating plasma is rather difficult due to the possible complications in the

hydrodynamic velocity distribution of the imploding ions. It should be mentioned, however, that the estimated ion-ion collision time at stagnation is significantly shorter than the stagnation period and the mean free path for collisions is smaller than the plasma diameter, which tends to cause fast ion thermalization. For example, the collision time between $Z=5$ ions (based on Refs. [7,8,9] this is the minimum Z of the ions reaching the axis) at the relevant ion density is < 0.5 ns, and the m.f.p. (based on the final implosion ion velocity obtained from the present data) is < 0.1 mm.

As is commonly known it is rather difficult to study the particle thermalization from measurements of the particle velocity distribution, because of the ambiguities in discriminating the thermal velocities from the hydrodynamic velocities. The present data thus offer no information on the various components of the ion velocity distributions. The data, however, demonstrate clearly that the H-like ions lose most of their kinetic energy before recombining into lower charge state ions and before the electrons cool down sufficiently to terminate the H-like emission. Between $t=-4$ to $t=+6$ ns, the ions are seen (Figure 4) to lose a kinetic energy of 2.1 keV/ion. The ion energy loss in the plasma can only be transferred to the plasma electrons, which in turn lose the energy through radiation, ionizations, and thermal convection to the neighboring colder plasmas.

Our current modeling of the data is intended to obtain estimates of the various contributions to the plasma heating at stagnation. To this end, the energy losses of the plasma at stagnation are calculated and compared to the energy deposition by the imploding ions. For the energy-loss estimate, collisional-radiative and radiation-transport calculations are performed in order to determine the radiation and ionization energy losses and the ion number in the stagnating plasma as a function of time. The use of the electron density obtained from the satellite ratios (as mentioned above) in these calculations is of high importance for reducing the modeling uncertainties. Also in these calculations use is made of the absolute intensities of both the optically thin and thick lines, as well as the absolute continuum emission above the H-like edge (determined from the Ross-filter measurements). In addition, it will be verified that the modeling is consistent with the other observations such as the pinhole photography (which gives the plasma dimension) and the total radiated x-ray power.

The resulting time dependent energy loss per ion in the plasma will be compared to the observed energy deposition per ion that is shown in Figure 4. Such a comparison, together with the estimates of the thermal convection, may be useful for examining whether ohmic heating or $J \times B$ work contributed an additional energy to the stagnating plasma.

It is noteworthy to mention that for z locations for which the stagnating plasma is seen to emit He-like emission prior to the appearance of H-like emission, the He-like ion

kinetic energy is studied from the Doppler contribution to the spectral profile of the intercombination line (which is optically thin in our experiments). The modeling performed is planned to also make use of these measurements.

ACKNOWLEDGEMENTS

The authors acknowledge valuable critical discussions with J.P. Apruzese, J.E. Bailey, R.A. Comisso, J. Davis, C. Deeney, T. Mehlhorn, W. Thornhill, A.L. Velikhovich, and K.G. Whitney. We are indebted to P. Meiri for his highly skilled technical assistance.

This work was supported in part by the German-Israeli Project Cooperation Foundation (DIP), by Sandia National Laboratories (USA), and by the Israeli Science Foundation.

REFERENCES

- [1] T.W.L. Sanford et al., Dynamics of a high-power aluminum-wire array Z-pinch implosion, *Phys. Plasmas* **4**, 2188 (1997).
- [2] K.L. Wong et al., Spectroscopic Characterization of Argon-Neon Z-Pinch Plasma at Stagnation, *Phys. Rev. Lett.* **80**, 2334 (1998).
- [3] E.Y. Yadlowsky et al., High resolution measurements of ion temperatures in z-pinch plasmas, *J. Appl. Phys.* **92**, 3458 (2002).
- [4] E. Kroupp et al., Investigation of Ne IX and Ne X line emission from dense plasma using Ross-filter systems, *J. Appl. Phys.* **92**, 4947 (2002).
- [5] L.A. Vainshtein et al., Wavelengths and Transition Probabilities of Satellites to Resonance Lines of H- and He-like Ions, *ADNDT* **21**, 49 (1978).
- [6] J.F. Seely, Dielectronic Satellite Spectra to Lyman-Alpha, *ADNDT* **26**, 138 (1981).
- [7] M. E. Foord et al., Particle velocity distributions and ionization processes in a gas-puff Z pinch, *Phys. Rev. Lett.* **72**, 3827 (1994).
- [8] G. Davara et al., Spectroscopic determination of the magnetic field distribution in an imploding plasma, *Phys. Plasmas* **5** (1), 1068 (1998).
- [9] L. Gregorian et al., Use of emission-line intensities for a self-consistent determination of the particle densities in a transient plasma, *Phys. Rev. E* **67**, 016404 (2003).